RHEUMATOLOGY

Rheumatology 2021;60:4508–4519
doi:10.1093/rheumatology/keab022
Advance Access publication 26 January 2021

Original article

Glycolysis-derived acidic microenvironment as a driver of endothelial dysfunction in systemic sclerosis

Elena Andreucci [1], Francesca Margheri [1], Silvia Peppicelli[1], Francesca Bianchini[1], Jessica Ruzzolini[1], Anna Laurenzana[1], Gabriella Fibbi[1], Cosimo Bruni [2], Silvia Bellando-Randone[2], Serena Guiducci[2], Eloisa Romano[2], Mirko Manetti [3], Marco Matucci-Cerinic[2] and Lido Calorini[1,4]

Abstract

Objectives. SSc is an autoimmune disease characterized by peripheral vasculopathy and skin and internal organ fibrosis. Accumulating evidence underlines a close association between a metabolic reprogramming of activated fibroblasts and fibrosis. This prompted us to determine the metabolism of SSc dermal fibroblasts and the effect on the vasculopathy characterizing the disease.

Methods. A Seahorse XF96 Extracellular Flux Analyzer was used to evaluate SSc fibroblast metabolism. *In vitro* invasion and capillary morphogenesis assays were used to determine the angiogenic ability of endothelial cells (ECs). Immunofluorescence, flow cytometry and real-time PCR techniques provided evidence of the molecular mechanism behind the impaired vascularization that characterizes SSc patients.

Results. SSc fibroblasts, compared with controls, showed a boosted glycolytic metabolism with increased lactic acid release and subsequent extracellular acidification that in turn was found to impair EC invasion and organization in capillary-like networks without altering cell viability. A molecular link between extracellular acidosis and endothelial dysfunction was identified as acidic ECs upregulated MMP-12, which cleaves and inactivates urokinase-type plasminogen activator receptor, impairing angiogenesis in SSc. Moreover, the acidic environment was found to induce the loss of endothelial markers and the acquisition of mesenchymal-like features in ECs, thus promoting the endothelial-to-mesenchymal transition process that contributes to both capillary rarefaction and tissue fibrosis in SSc.

Conclusion. This study showed the relationship of the metabolic reprogramming of SSc dermal fibroblasts, extracellular acidosis and endothelial dysfunction that may contribute to the impairment and loss of peripheral capillary networks in SSc disease.

Key words: systemic sclerosis, glycolysis, extracellular acidosis, angiogenesis

CLINICAL SCIENCE

Rheumatology key messages

- Systemic sclerosis fibroblasts are characterized by an increased glycolytic metabolism and subsequent extracellular medium acidification.
- Extracellular acidosis of scleroderma tissues impairs endothelial cell migration and organization in capillary-like networks.
- Extracellular acidosis impairs angiogenesis by inducing MMP-12-derived uPAR cleavage and the endothelial-to-mesenchymal transition process in endothelial cells.

[1]Department of Experimental and Clinical Biomedical Sciences 'Mario Serio', Section of Experimental Pathology and Oncology, [2]Department of Experimental and Clinical Medicine, Division of Rheumatology, [3]Department of Experimental and Clinical Medicine, Section of Anatomy and Histology and [4]Centre for Research, Knowledge Transfer and Higher Education, University of Florence, Florence, Italy

Submitted 13 August 2020; accepted 6 January 2021

Correspondence to: Elena Andreucci, Department of Experimental and Clinical Biomedical Sciences 'Mario Serio', Section of Experimental Pathology and Oncology, University of Florence V.le Morgagni, 50-50134 Florence, Italy. E-mail: e.andreucci@unifi.it

Introduction

SSc is a chronic disabling autoimmune disorder characterized by widespread tissue fibrosis and vascular abnormalities [1–4]. Despite being a rare disease, SSc has high morbidity and mortality [5]. Autoimmunity/inflammation, fibrosis and vascular rarefaction represent the pathogenic triad of SSc [3]. A fibroproliferative and destructive vasculopathy is considered one of the earliest disease manifestations, even preceding fibrosis [2, 6]. Among them, endothelial cell (EC) activation,

apoptosis and dysregulation of the pericyte–EC crosstalk have been described [4, 7].

Emerging evidence has positioned the glycolytic metabolism as a key factor that may promote fibrosis in different diseases. In addition, glycolysis plays an essential role in rheumatic diseases such as RA, SLE and OA [1, 8–10]. Of note, glycolytic metabolism appears to be closely associated with myofibroblastic activation and a lung profibrotic phenotype, suggesting that pulmonary fibrosis—and likely other fibrotic conditions—may be characterized by glycolytic dysregulation [11–13]. Moreover, in an experimental model of SSc, the aerobic glycolytic shift was suggested to be an important mechanism to ensure fibroblast survival [14]; also, keloid scar fibroblasts, which share many characteristics with SSc fibroblasts, use aerobic glycolysis as their primary energy source [15].

In line with this evidence, the aim of our work was to evaluate for the first time the glycolytic metabolism of SSc dermal fibroblasts and the effect of this metabolic dysregulation on EC angiogenic potential.

Materials and methods

Cell culture

Normal human dermal fibroblasts (Sigma-Aldrich, Milan, Italy) isolated from normal adult skin were used as control cells and compared with previously isolated SSc fibroblasts (SSc1 and SSc2) from affected dorsal skin of the hands of two diffuse SSc patients attending the Rheumatology Division of Careggi Hospital in Florence, Italy (SSc1: male, 52 years old, disease duration 15 years; SSc2: female, 65 years old, disease duration 9 years) [16]. Control and SSc fibroblasts were maintained in culture between the 3rd and 10th passage in DMEM 4.5 g/l glucose and 2 mM L-glutamine supplemented with 10% foetal bovine serum (FBS; Euroclone, Milan, Italy) and cryopreserved in liquid nitrogen. ECs used in this work were endothelial colony-forming cells, as they are an EC type endowed with intrinsic angiogenic capacity and the ability to contribute to vascular repair and *de novo* blood vessel formation [17]. ECs were isolated and characterized as previously described [18] and grown in the EGM-2 EC growth medium-2 Bullet Kit (Lonza, Basel, Switzerland) onto Attachment Factor Solution–coated dishes (Sigma-Aldrich). While the spontaneous acidification of SSc fibroblast media was measured as described in the 'Lactate and pH measurement' section, the chemically induced acidic extracellular microenvironment under which ECs were cultivated was obtained *in vitro* by 1 N hydrogen chloride (HCl) administration directly in complete EC culture medium to reach pH 7.0 and 6.7 in the presence or absence of 10 mM lactate (Sigma-Aldrich) and pH monitored using an Orion 520A1 pH meter (Thermo Fisher Scientific, Waltham, MA, USA).

Western blotting

Fibroblasts were lysed in radioimmunoprecipitation assay lysis buffer (Merck Millipore, Milan, Italy) containing Pierce Protease Inhibitor Tablets (Thermo Fisher Scientific). Equal amounts of protein were separated in Laemmli buffer on 8–12% (v/v) SDS-PAGE gel (Thermo Fischer Scientific) and transferred to a polyvinylidene fluoride membrane. Membranes were blocked and probed overnight at 4°C with anti-COL1A1 and anti-β-actin (Santa Cruz Biotechnology, Heidelberg, Germany) antibodies. Membranes were incubated 1 h at room temperature with goat anti-rabbit IgG Alexa Flour 750 antibody (Invitrogen, Carlsbad, CA, USA) and visualized by the Odyssey Infrared Imaging System (LI-COR Biosciences, Lincoln, NE, USA).

Cell viability

Trypan blue exclusion test

Fibroblasts were grown up to 70% confluence, then medium was removed and replaced with glucose-free medium. Twenty-four hours later, 20 μl of cell suspension were incubated with an equal volume of trypan blue solution (Sigma-Aldrich). Viable (trypan blue negative) and non-viable (trypan blue positive) cells were counted on a light microscope using a dual-chamber haemocytometer.

Annexin V/PI flow cytometer assay

ECs were grown for 24, 48 and 72 h at standard pH 7.4 and acidic pH 7.0 and 6.7 in the presence or absence of 10 mM lactate. At each time point, 1×10^5 cells/tube were harvested with Accutase (Eurolone), incubated 15 min at 4°C in the dark with 100 μl annexin binding buffer [100 mM 4-(2-hydroxyethyl)-1-piperazineethanesulfonic acid (HEPES), 140 mM sodium chloride, 25 mM calcium chloride, pH 7.4], 1 μl of 100 μg/ml propidium iodide (PI; Sigma-Aldrich) working solution and 5 μl annexin V fluorescein isothiocyanate (FITC)-conjugated (Immunotools, Friesoythe, Germany). Samples were analysed with a BD FACS Canto II (BD Biosciences, Franklin Lakes, NJ, USA). Cellular distribution depending on annexin V and/or PI positivity allowed the measurement of the percentage of viable cells (annexin V and PI negative), early apoptosis (annexin V positive and PI negative), late apoptosis (annexin V and PI positive) and necrosis (annexin V negative and PI positive).

Seahorse analysis

A total of 8×10^3 fibroblasts were seeded onto XF96 Seahorse microplates and evaluated with a Seahorse XF96 Extracellular Flux Analyzer (Seahorse Bioscience, Billerica, MA, USA) for their glycolytic and respiratory metabolism using the Glycolysis Stress Test and the Cell Mito Stress Test Kits (Agilent Technologies, Santa Clara, CA, USA), according to the manufacturer's instruction. All the experiments were performed at 37°C and normalized via cell protein measure with a Pierce BCA Protein Assay Kit (Thermo Fisher Scientific). The Seahorse XF Report Generator automatically calculated

the parameters from wave data that were exported to GraphPad Prism software (GraphPad Software, San Diego, CA, USA).

MMP-12 detection in patient-derived sera

MMP-12 levels in patient-derived sera were measured by using a Human MMP-12 ELISA Kit (Thermo Fisher Scientific), according to the manufacturer's instructions. Data were presented as ng/ml.

Real-time PCR

Total RNA isolated from fibroblasts and ECs was prepared using Tri Reagent (Sigma-Aldrich), agarose gel checked for integrity and reverse transcribed with iScript cDNA Synthesis Kits (Bio-Rad, Milan, Italy) according to the manufacturer's instructions. Selected genes were evaluated by real-time RT-PCR with a CFX96 Real-Time PCR System (Bio-Rad). The fold change was determined by the comparative Ct method using β2-microglobulin and β-actin as the reference genes. Amplification was performed with a PCR setting of 40 cycles of 95°C for 10 s and 60°C for 30 s using SsoAdvanced Universal SYBR Green Supermix (Bio-Rad). Primer sequences (Tema Ricerca, Bologna, Italy) are listed in Table 1.

Lactate and pH measurement

A D-Lactate Colorimetric Assay Kit (BioVision, Milpitas, CA, USA) was used according to the manufacturer's instructions to measure lactate production in fibroblast conditioned media (CM). Data normalization was obtained by directly counting the number of cells to get a final result of lactate production (in nM) by 1×10^5 cells. To test the spontaneous acidification and measure the pH of the fibroblast culture medium, the same number of control and SSc fibroblasts were plated to reach 80% confluence and allowed to adhere to the tissue culture dish. Then standard growth medium was replaced with DMEM 4.5 g/l glucose, 2 mM L-glutamine and 10% FBS without sodium bicarbonate. Cells were incubated overnight in a humidified atmosphere at 10% carbon dioxide and the pH was measured using an Orion 520A1 pH meter (Thermo Fisher Scientific).

Invasion and chemo-invasion assays

The 12 mm diameter Millicell Cell Culture Inserts (Merck Millipore) were mounted in 24-well plates and 2.5×10^4 ECs plated in 400 μl of their growth medium on 0.25 μg/μl Matrigel pre-coated polycarbonate filters with 8 μm pore size. ECs were left migrate for 6 h at 37°C towards the lower compartment filled with 400 μl of complete EGM-2 medium. After 1 h of fixation in methanol at 4°C, non-invading cells on the upper side of the filters were mechanically wiped off with a cotton swab, while invasive cells on the lower side of the filters were stained with a Diff-Quick kit (BD Biosciences), then visualized and counted using an optical microscope. The chemo-invasion assay was performed the same as the invasion assay described above, with the difference that the lower compartment was filled with CM from controls and SSc fibroblasts.

Capillary morphogenic assay

A total of 0.2×10^5 ECs/well were plated on 96-well plates pre-coated with 50 μl Matrigel (Miscio Rappresentanze, Perugia, Italy) and cultured in FBS-free EGM-2 medium. Cells were incubated for 6 h at 37°C and pictures acquired using an EVOS optical microscope (Thermo Fisher Scientific). The angiogenesis analyser tool of ImageJ software, by measuring the number of nodes, segments, meshes and junctions per field, provided the statistical analysis for each experimental condition tested. ECs were tested for capillary morphogenic assay upon acidic treatment (see the Cell culture section) or in the presence of CM derived from controls and SSc fibroblasts or in the presence of sera collected

Table 1 List of primers used for real-time PCR analysis

Gene	Forward (5′–3′)	Reverse (5′–3′)
β2-microglobulin	GCCGTGTGAACCATGTGACT	GCTTACATGTCTCGATCCCACTT
β-actin	TCGAGCCATAAAAGGCAACT	CTTCCTCAATCTCGCTCTCG
PDK1	CCAAGACCTCGTGTTGAGACC	AATACACGTCTCAGGTCTCCTTGG
PDP2	TAGGCCAACCTTTGTTTCACCA	AGACCCTCACAACAAAAGCCT
LDHA	AGGGAATGTACGGCATTGAG	CCTCATCGTCCTTCAGCTTC
VE-cadherin	TCGCTGTTGTCACATCTCAGGGAA	TGACTGATGCCACTTCTCCAAGGT
uPAR	GGTCACCCGCCGCTG	CCACTGCGGGTACTGGACA
MMP-12	TGCTGATGACATACGTGGCA	AGGATTTGGCAAGCGTTGG
TGF-β	GACTACTACGCCAAGGAGGTCA	TGCTGTGTGTACTCTGCTGCTTTGAAC
α-SMA	CTGTTCCAGCCATCCTTCAT	CCGTGATCTCCTTCTGCATT
COL1A1	CTGTTCTGTTCCTTGTGTAACTGTGTT	GCCCCGGTGACACATCAA
Twist	CGGGAGTCCGCAGTCTTA	TGAATCTTGCTCAGCTTGTC
Snail	CCCAGTGCCTCGACCACTAT	CCAGATGAGCATTGGCAG
Zeb1	GGCAACCAGTTCTCCTCAGG	TTGGATGCAAGATTGGCTTG
Zeb2	GAGCACATCAAGTACCGCCA	ACCTGCTCCTTGGGTTAGCA

from a healthy donor and four SSc patients (age, sex, disease duration and inflammatory markers for each patient are reported in Supplementary Table S1, available at *Rheumatology* online).

Immunofluorescence

ECs were grown on glass coverslips in six-well plates in standard or acidified medium in the presence or absence of 10 mM lactate for 24 h. ECs were fixed for 30 min at 4°C with 3.7% paraformaldehyde and permeabilized for 15 min with PBS 0.1% Triton X-100 at room temperature. After a 1 h incubation in blocking buffer (0.1% Triton X-100 and 5.5% horse serum PBS), cells were stained with anti-urokinase-type plasminogen activator receptor (uPAR)MON-R4 antibody (Thermo Fisher Scientific) for 1 h at room temperature and then 45 min at room temperature in the dark with Cy3-conjugated anti-mouse antibody (Invitrogen, Carlsbad, CA, USA). Following the 20 min nuclei staining with DAPI (Thermo Fisher Scientific) at room temperature in the dark, cells were mounted onto glass slides and visualized with at Eclipse TE2000-U confocal microscope (Nikon, Tokyo, Japan). ImageJ software was used to calculate the corrected total cellular fluorescence (CTCF): CTCF = integrated density − (cell area × fluorescence average of background readings).

Flow cytometer

A total of 2×10^5 cells/tube of ECs were harvested by using Accutase (Euroclone, Milan, Italy), permeabilized with 0.25% Triton X-100 PBS, stained 1 h at 4°C with anti-uPAR MON-R4 (Thermo Fisher Scientific) and 1 h in the dark at 4°C with secondary FITC-conjugated antibody (Merck Millipore). For each sample, 1×10^4 events were analysed using an FACS Canto II (BD Biosciences).

Statistical analysis

The experiments were performed at least four times for a reliable application of statistics. All samples used were included in the statistical analysis. Statistical analysis was performed by *t*-test, one-way analysis of variance (ANOVA) and two-way ANOVA with GraphPad Prism 6 software (GraphPad Software), as specified in each figure legend.

Results

SSc fibroblasts exploit a higher glycolytic metabolism compared with normal fibroblasts

In this work, dermal fibroblasts derived from patients with diffuse cutaneous SSc (SSc1 and SSc2) were compared with commercially available normal dermal fibroblasts (CTRL). An increased expression of type I collagen characterized the activated phenotype of SSc fibroblasts (Fig. 1a). By culturing all types of fibroblasts for 24 h in a glucose-free medium, we observed that ∼60% of SSc1 and ∼80% of SSc2 fibroblasts underwent cell death, while CTRL cells did not show any cell viability impairment (Fig. 1b), showing a glucose dependence of SSc fibroblasts. By checking their metabolism with an XFe96 bioanalyzer (Seahorse Bioscience), we found a clear promotion of glycolysis counterbalanced by a reduction in respiration in SSc fibroblasts. Indeed, when assessed with the glycolysis stress test, SSc fibroblasts showed an increased glycolysis and glycolytic capacity compared with controls (Fig. 1c, upper) and significantly reduced basal respiration and spare respiratory capacity when subjected to the Mito stress test (Fig. 1c, lower). Real-time PCR analysis confirmed their metabolic shift towards glycolysis, since the pyruvate dehydrogenase kinase 1 (PDK1):pyruvate dehydrogenase phosphatase 2 (PDP2) ratio and lactate dehydrogenase A (LDHA) were significantly up-regulated in SSc fibroblasts (Fig. 1d). Accordingly, the measurement of pH and lactate content in CM revealed that SSc1 and SSc2 fibroblasts produced a two- to three-fold increased amount of lactic acid compared with control cells (Fig. 1e). Together, a dynamic measure of metabolism and the evaluation of glycolytic markers clearly demonstrated the glycolytic addiction of SSc fibroblasts.

Reduced pH impairs EC activities

As a direct consequence of the high SSc glycolytic activity, in particular the lactic acid release, extracellular pH of the SSc microenvironment undergoes progressive acidification. Therefore we wondered if the acidic microenvironment could be a cause of the impaired EC activity that characterizes SSc lesions. In accordance with the pH values of spontaneously acidified SSc fibroblast media [pH 6.8 (S.D. 0.1) and 6.9 (S.D. 0.1) *vs* 7.3 (S.D. 0.1) of control fibroblasts, see Fig. 1e], we cultivated ECs under a non-physiological acidic pH of 7.0 and 6.7 (S.D. 0.1), obtained by HCl administration directly into the culture medium (see the Cell culture paragraph in the Materials and methods section), in order to mimic the spontaneous acidified tissue microenvironment caused by the altered metabolism of SSc fibroblasts. A significant reduction of EC tube formation (in terms of both lumen and network formation) was observed at acidic pH 7.0 and was further strengthened at pH 6.7, as reported by the statistical analysis of the angiogenic parameters of nodes, segments, meshes and junctions reported by the angiogenesis analyser of ImageJ software (Fig. 2a). It should be noted that lactate caused a further impairment of capillary morphogenesis under acidic pH 7.0, but by lowering pH to 6.7, this synergistic effect was no longer visible. EC invasion was significantly decreased under acidic pH 6.7, either in the presence or absence of lactate (Fig. 2b). We ascertained that these effects were not a result of acidosis-induced cell death. The annexin V/PI flow cytometer assay revealed that acidic conditioning of ECs up to 72 h, in the presence or absence of lactate, did not alter their viability (Fig. 2c). Indeed, tube formation and invasion abilities were completely restored by increasing pH to 7.4 (Supplementary Fig. S1a–b, available at *Rheumatology*

Fig. 1 Enhanced glycolytic metabolism of SSc fibroblasts

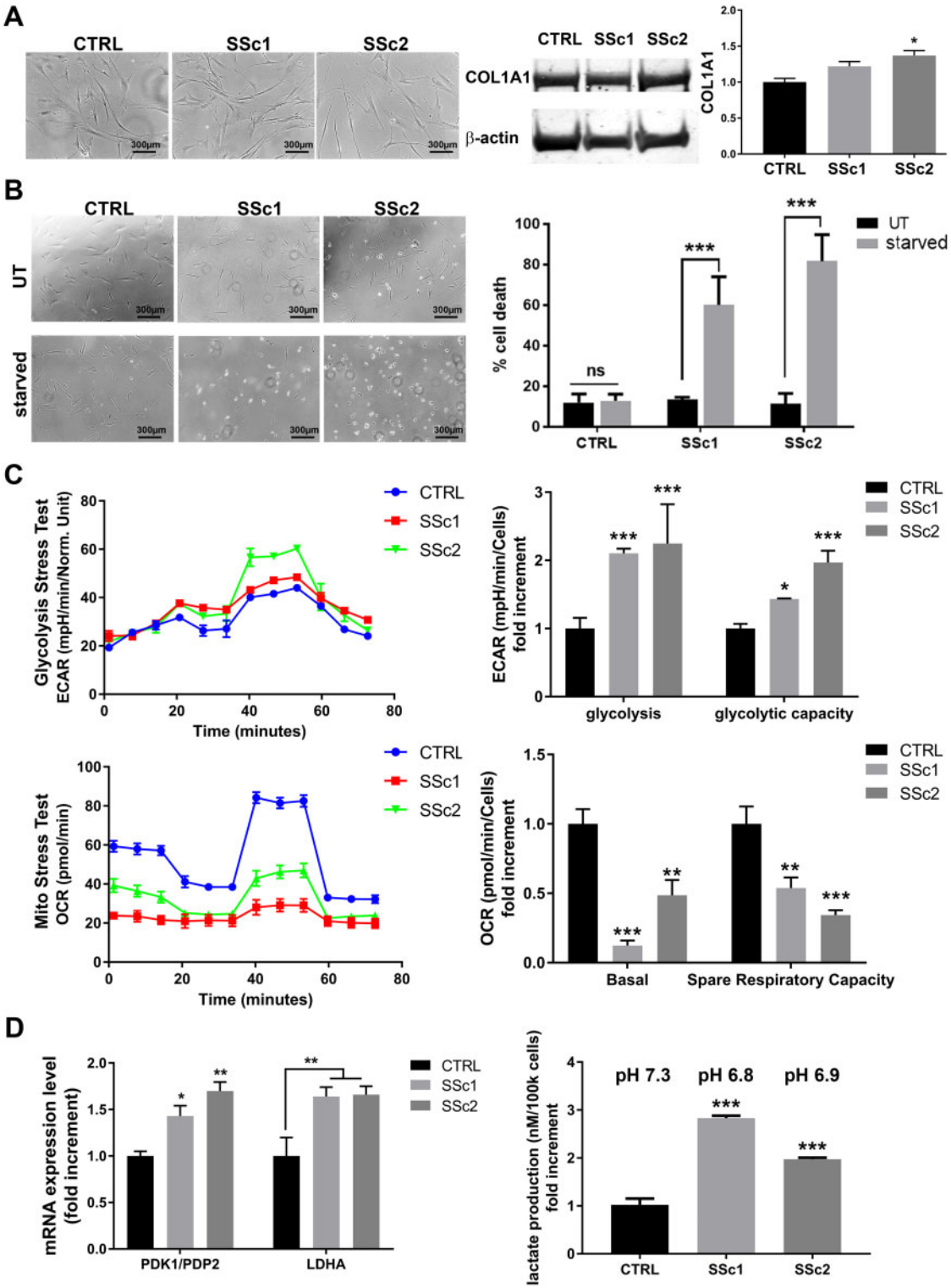

(**A**) Morphology and type I collagen expression of control and SSc fibroblasts (scale bar: 300 μm). One-way ANOVA, Tukey's multiple comparisons test. (**B**) Representative pictures and trypan blue assay of control and SSc fibroblasts after 24 h of glucose starvation. Two-way ANOVA, Tukey's multiple comparisons test. (**C**) Glycolysis (upper) and Mito (lower) stress tests (two-way ANOVA, Sidak's multiple comparisons test). (**D**) Real-time PCR analysis of metabolic markers in control and SSc fibroblasts (two-way ANOVA, Tukey's multiple comparisons test). (**E**) Lactate and pH measures in CM of control and SSc fibroblasts. One-way ANOVA, Dunnett's multiple comparisons test.

Fig. 2 Acidic microenvironment exerts anti-angiogenic effects

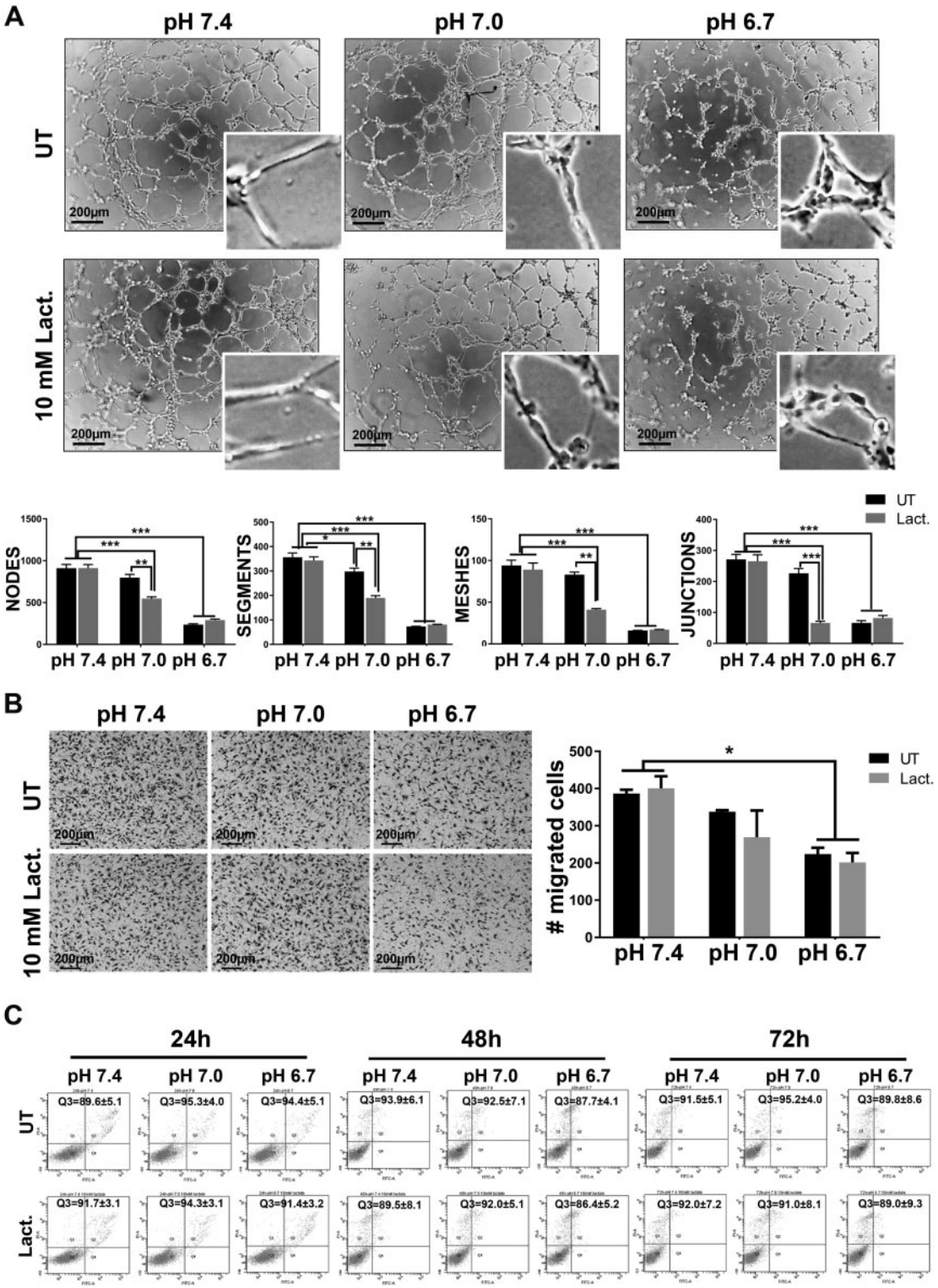

Representative pictures and quantification chart of (**A**) EC tube formation (scale bar: 200 μm) and (**B**) EC invasion through Matrigel (scale bar: 200 μm) under standard (pH 7.4) or acidic (pH 7.0 and 6.7) conditions in the presence or absence of 10 mM lactate. Two-way ANOVA, (**A**) Sidak's and (**B**) Tukey's multiple comparisons test. (**C**) Representative plots of annexin V/PI assay of ECs exposed to standard (pH 7.4) or acidic (pH 7.0 and 6.7) conditions in the presence or absence of 10 mM lactate for 24–72 h. Not significant, two-way ANOVA, Tukey's multiple comparisons test.

FIG. 3 SSc-derived CM impairs EC angiogenic activities

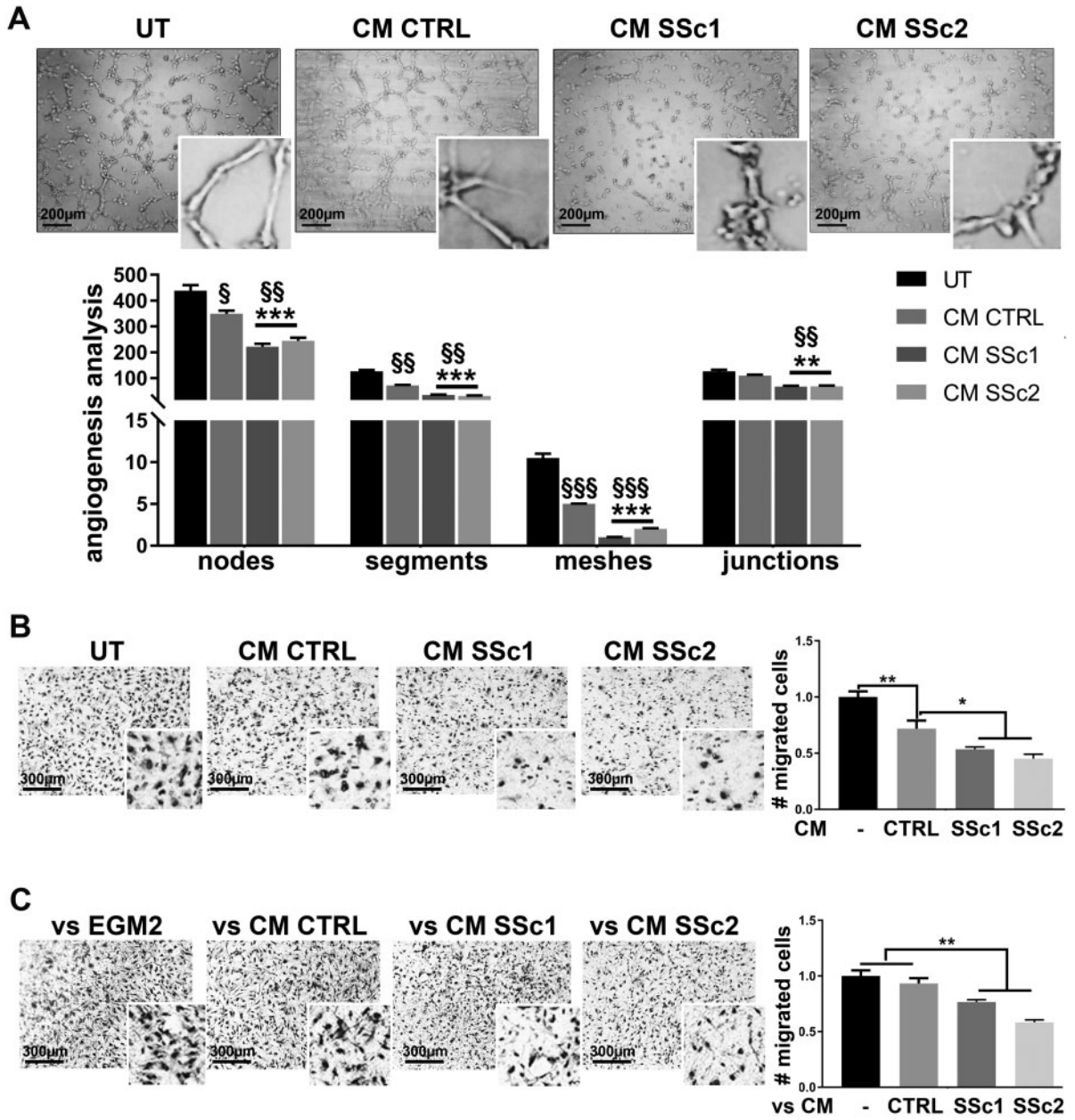

Representative pictures and quantitative analysis of (**A**) EC tube formation (scale bar: 200 μm, two-way ANOVA, Tukey's multiple comparisons test) and (**B**) EC invasion through Matrigel (scale bar: 300 μm, one-way ANOVA, Tukey's multiple comparisons test) in EGM-2 medium or CM derived from control or SSc fibroblasts (* *vs* CM CTRL; § *vs* EGM-2 medium). (**C**) Representative pictures and quantitative analysis of the EC chemo-invasion assay towards EGM-2 medium or CM derived from control or SSc fibroblasts (scale bar: 300 μm; one-way ANOVA, Tukey's multiple comparisons test).

online). Accordingly, VE-cadherin, a marker of EC stability, was down-regulated under acidosis but re-expressed at control or even higher levels when the normal pH condition was restored (Supplementary Fig. S1c, available at *Rheumatology* online). Acidic CMs derived from SSc1 and SSc2 fibroblasts [pH 6.8 and 6.9 (S.D. 0.1), respectively, as shown in Fig. 1e] compared with CMs derived from control fibroblasts [pH 7.3 (S.D. 0.1)] decreased *in vitro* EC tube formation (Fig. 3a) and invasion (Fig. 3b). SSc CM also impaired *in vitro* EC chemoattraction while control CM did not induce any variation compared with the untreated condition (Fig. 3c), meaning that even EC recruitment in SSc affected areas is likely impaired.

FIG. 4 The MMP-12-mediated uPAR cleavage anti-angiogenic mechanism is up-regulated under acidic conditions

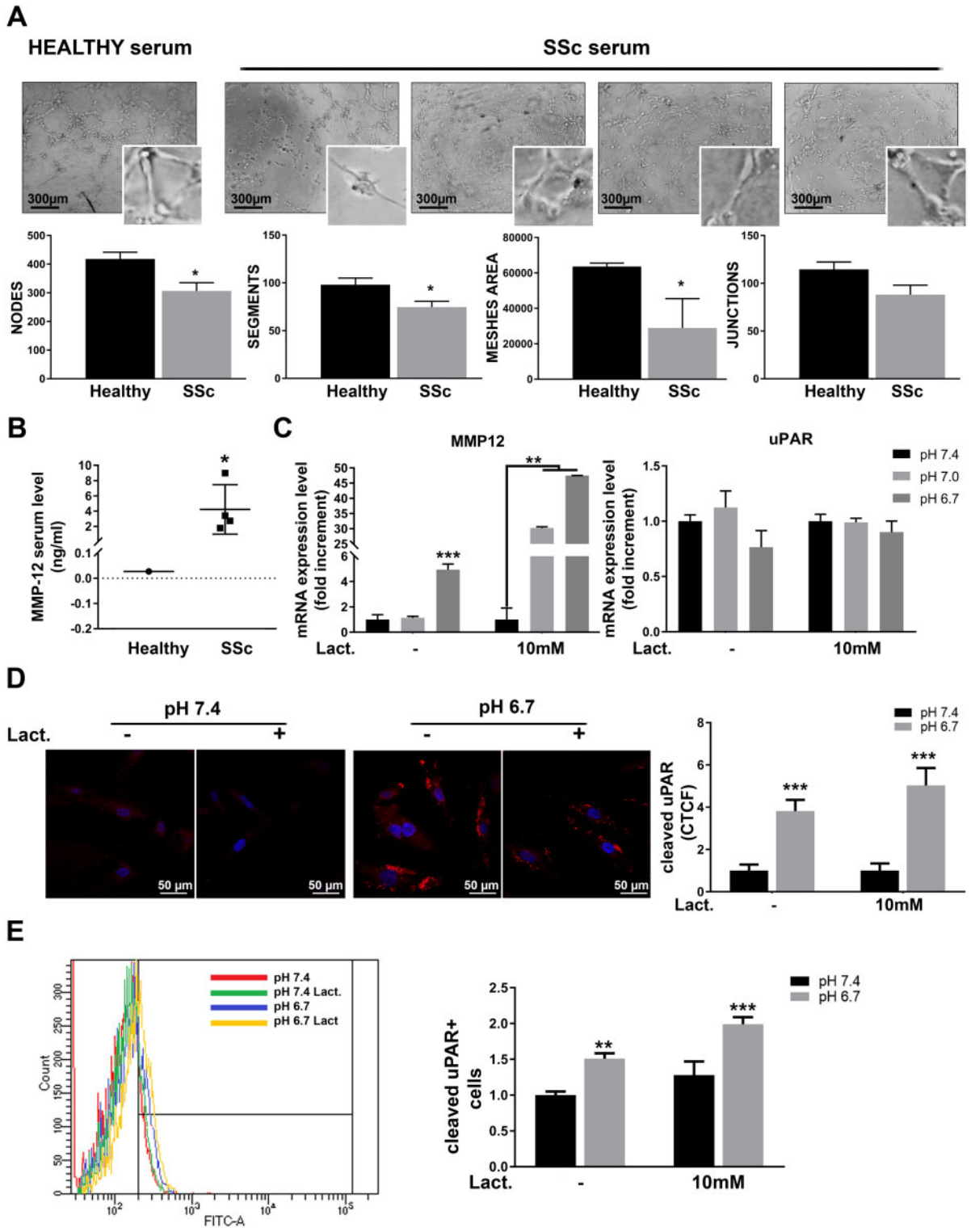

(**A**) EC tube formation in the presence of one healthy and four SSc sera. Scale bar: 300 µm, *t*-test. (**B**) MMP-12 ELISA test of the one healthy and the four SSc sera used in (A) (*t*-test). (**C**) Real-time PCR analysis of MMP-12 and uPAR in ECs exposed to standard and acidic conditions in the presence or absence of 10 mM lactate. Two-way ANOVA, Tukey's multiple comparisons test. (**D**) Immunofluorescence (scale bar: 50 µm, two-way ANOVA, Sidak's multiple comparisons test) and (**E**) flow cytometry (two-way ANOVA, Sidak's multiple comparisons test) of cleaved uPAR in EC exposed to standard or acidic conditions in the presence or absence of 10 mM lactate.

Fig. 5 Acidic ECs undergo endoMT

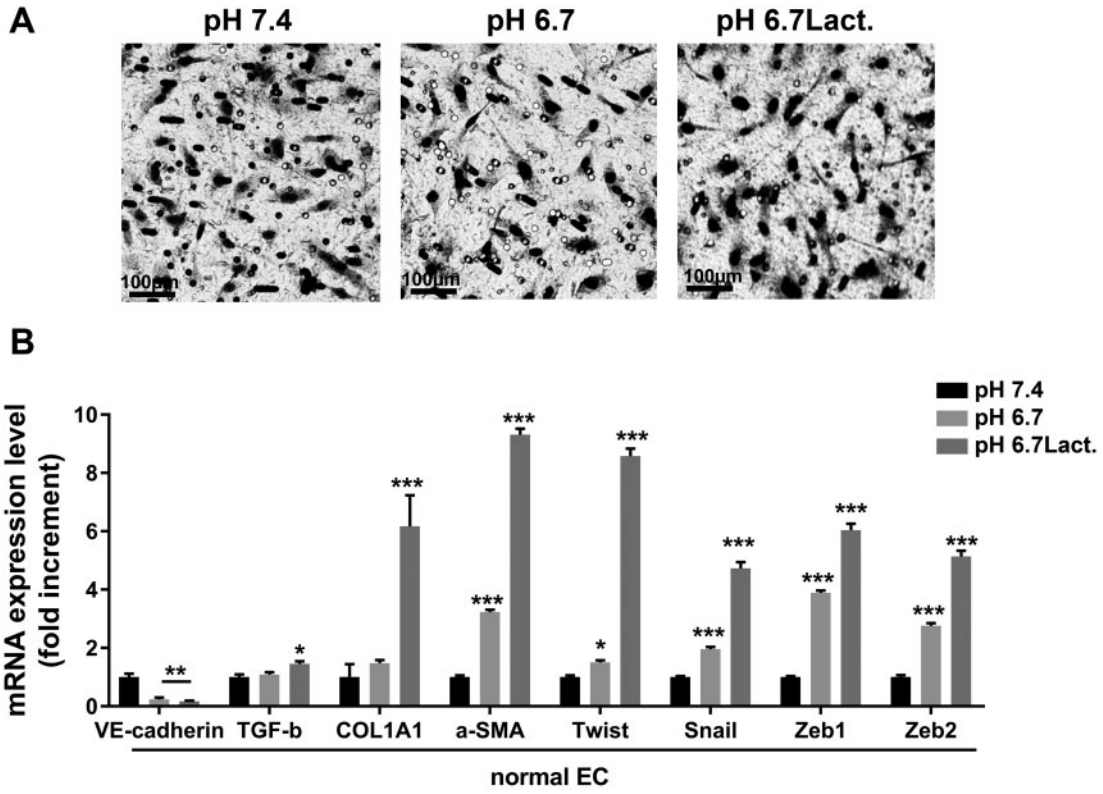

(**A**) Representative pictures of morphology (scale bar: 100 μm) and (**B**) real-Time PCR analysis of endoMT markers of ECs exposed to the standard condition (pH 7.4), acidosis (pH 6.7) or lactic acidosis (pH 6.7Lact). Two-way ANOVA, Dunnett's multiple comparisons test.

Together these findings suggest that SSc fibroblast glycolytic addiction and activity may contribute to the impairment of angiogenesis.

A molecular mechanism linking extracellular acidosis and endothelial dysfunction

Four SSc sera compared with one healthy donor serum were tested *in vitro* for their ability to impair EC tube formation. Defective capillary-like networks were observed when ECs were exposed to the SSc sera compared with the healthy one, with a significantly decreased number of nodes, segments and meshes, and also a reduction (even though not significant) in the number of junctions (Fig. 4a). SSc sera showed significantly higher levels of MMP-12 compared with the healthy serum (Fig. 4b). We have already reported that MMP-12 is significantly up-regulated in serum of SSc patients compared with healthy people [19], representing one of the mechanisms involved in SSc vascular alterations. MMP-12 plays a key role in angiogenesis inhibition, as it drives uPAR cleavage, thus preventing the pro-angiogenic activity of uPAR signalling [16, 20]. As we already reported, uPAR is indeed indispensable for EC-driven angiogenesis [21]. What is not yet known is whether the acidic microenvironment promotes this MMP-12-mediated uPAR cleavage leading to angiogenesis inhibition. In Fig. 4c (left panel), we show that MMP-12 mRNA expression was significantly up-regulated in ECs exposed to pH 6.7 and the increase was further strengthened in the presence of lactate. While uPAR mRNA expression levels did not significantly vary under acidosis and lactic acidosis compared with the standard pH condition (Fig. 4c, right panel), the cleaved uPAR protein level was significantly increased in ECs exposed to acidosis and lactic acidosis than in standard pH. Accordingly, by confocal microscopy we observed an ∼4-fold increment, compared with controls, of cleaved uPAR in acidic ECs that was further enhanced up to ∼5-fold under lactic acidosis (Fig. 4d); accordingly, by flow cytometer analysis we found a similar trend, with an ∼1.5- and ∼2-fold increase of cleaved uPAR levels in ECs under acidosis and lactic acidosis, respectively (Fig. 4e).

Thus we may propose a scenario in which extracellular acidosis caused by the SSc fibroblast glycolytic addiction promotes EC dysregulation and angiogenesis impairment through MMP-12-mediated uPAR cleavage.

The acidic microenvironment drives endothelial-to-mesenchymal transition (endoMT)

We further investigated the fate of ECs exposed to extracellular acidosis and displaying an impaired ability to perform angiogenesis. Acidic ECs acquired a

mesenchymal-like morphology (Fig. 5a) and showed a significant down-regulation of the endothelial marker VE-cadherin, associated with a higher expression of the myofibroblast markers TGF-β, type I collagen, α-smooth muscle action (SMA) and the transcription factors Twist, Snail, Zeb1 and Zeb2 (Fig. 5b). This may look like an endoMT phenomenon, a trans-differentiation process in which ECs lose their specific markers and acquire, either totally or partially, a myofibroblast-like phenotype that is known to contribute to vascular dysfunction and dermal fibrosis in SSc [22–25].

The acidic microenvironment may thus contribute, by inducing endoMT, to the degenerative fibrotic and vasculopathic features of SSc.

Discussion

Our data clearly show that SSc dermal fibroblasts have an increased glycolytic metabolism causing extracellular acidification that deeply impairs EC angiogenic potential. It is well known that metabolic dysregulation can foster the progression of various types of diseases, including cancer and rheumatic diseases [1]. In particular, emerging evidence indicates that enhanced glycolysis may be associated with fibrotic remodelling of multiple organs and represents a necessary condition for the development and sustainment of pro-fibrotic myofibroblast differentiation [11, 26–29]. Here, although with the presence of some limitations, such as the limited number of SSc fibroblast lines and the comparison between patient-derived SSc fibroblasts with commercially available normal fibroblasts, we demonstrate that SSc fibroblasts show a selective glucose dependence and an increased glycolysis accompanied by a reduction in their respiratory capacity. Indeed, metabolomic profiling of SSc patients revealed that glycolysis and gluconeogenesis pathways are the most important pathways altered in dcSSc compared with lcSSc and a significant reduction in glucose serum levels along with disease progression was found [30]. Moreover, increased ^{18}F-fluorodeoxyglucose uptake has been reported in the skin and soft tissue calcinosis of SSc patients [1, 31, 32], as well as in patients affected by interstitial lung disease [33], which corroborates increased glucose use in such compromised tissues.

As a direct consequence of lactic acid release by the highly glycolytic SSc fibroblasts and also sustained by hampered removal, the tissue microenvironment inevitably becomes acidic, perturbing most of the adjacent cellular elements. This means that such altered metabolism causes a change in the local pH in the tissue around SSc fibroblasts, which falls into the non-physiological range of ∼7.0–6.7 (S.D. 0.1). Such pH modifications would be limited to the local SSc tissue microenvironment. It is known that fibroblasts are often exposed to metabolic acidosis, an important parameter of the local microenvironment found in several disorders such as inflammation, ischaemia and solid tumours. Strikingly, disease progression might be promoted by this 'new' metabolically altered microenvironment, as already shown for cancer, in which extracellular acidity reinforces their pro-tumoral effects in cancer-associated fibroblasts [34–36]. Thus our experiments meant to reproduce the likely *in vivo* situation in which local tissue acidosis/lactic acidosis would affect the physiological functions of other cell types around SSc fibroblasts, such as ECs. In line with the reduced human umbilical vein response to VEGF for cell proliferation and migration upon acidic exposure [37], we observed that acidosis per se and lactic acidosis are sufficient conditions to dramatically impair *in vitro* EC capillary network/lumen formation and invasion without altering cell viability. Tube formation and invasion were restored together with VE-cadherin expression with standard pH condition re-establishment. In accordance with our findings, potentiated angiogenic activity of human endothelial colony-forming cells that have undergone acidic preconditioning and then were re-exposed to standard pH has been shown [17, 38]. In apparent contrast with our observations, acidic pulmonary microvascular ECs increased network formation, although displaying impaired cell migration [39]. It is possible that organ specificity of ECs might be related to the different behaviour observed [40]. Indeed, lung endothelium is exposed to considerable luminal pH changes [41, 42] and thus pulmonary vascular ECs could be very adaptable cells to extracellular pH variations.

Looking for a molecular mechanism of angiogenesis inhibition by extracellular acidosis, we demonstrated that it promotes MMP-12 upregulation by ECs, likely accounting for the cleaved uPAR expressed by acidic ECs. In SSc sera and tissues, MMP-12 was found to be up-regulated [19] and may be responsible for endothelial uPAR cleavage and a consequent reduction of pro-angiogenic EC functions [16, 20]. Of note, uPAR can potentially mediate all the angiogenic phases [43, 44]. Recently the role of uPAR and other fibrinolytic regulators in SSc vasculopathy was reviewed [45]. There is evidence that uPAR-deficient mice develop peripheral vasculopathy and dermal and pulmonary fibrosis [46, 47]. Also, MMP-12-mediated uPAR cleavage has been implicated in the induction of endoMT in SSc dermal ECs [22]. Accordingly, we have shown that uPAR-deficient acidic ECs undergo endoMT, a process first proposed by Karasek in 2007 [25], by which ECs acquire myofibroblast-like features, detaching from the endothelial layer, becoming elongated and fusiform, losing their specific molecular markers (i.e. CD31/PECAM-1, von Willebrand factor and VE-cadherin) and acquiring, at the same time, mesenchymal markers (i.e. α-SMA, vimentin and type I collagen) [23]. EndoMT is a potential player in the pathogenesis of different fibrotic diseases and it seems to occur in the dermal endothelium of SSc patients, contributing to the development of skin fibrosis [22]. It is important to emphasize that the EC–myofibroblast transition does not need to be a total transdifferentiation, since a partial transition process may be enough for fibrogenesis initiation and progression [23].

Extracellular acidosis, by promoting the endoMT process, may provide an important contribution to SSc progression to tissue fibrosis. A connection between extracellular acidosis and fibrosis has also been found in cystic fibrosis [41, 48, 49] and idiopathic pulmonary fibrosis. In these diseases, pH measurement through the acidoCEST MRI technique showed that larger lung lesions correlate with higher lactic acid production and lower pH [50], in accordance with the metabolically induced local pH acidification that we propose for SSc tissues.

In conclusion, a chain of events may closely link the high glycolytic metabolism of SSc dermal fibroblasts and the resulting extracellular microenvironment acidification to the impairment of angiogenesis and EC–myofibroblast transdifferentiation, definitively fuelling the fibrotic process. These data suggest that a metabolic reconversion of fibroblasts might represent a novel therapeutic target in SSc patients.

Acknowledgements

Patient-derived SSc fibroblasts were isolated after approval of the local ethics committee and obtaining patient consent. Human sera were collected from patients involved in the European Scleroderma Trials and Research group (EUSTAR) upon approval of the Italian Ethics Committee 'Comitato Etico Area Vasta Centro'.

Funding: This work was financially supported by Ente Cassa di Risparmio di Firenze.

Disclosure statement: The authors declare that they have no conflicts of interest.

Data availability statement

The data underlying this article are available in the article and in its online supplementary material.

Supplementary data

Supplementary data are available at *Rheumatology* online.

References

1 Zhu H, Chen W, Liu D, Luo H. The role of metabolism in the pathogenesis of systemic sclerosis. Metabolism 2019;93:44–51.

2 Allanore Y, Simms R, Distler O *et al.* Systemic sclerosis. Nat Rev Dis Primer 2015;1: 15002.

3 Varga J, Trojanowska M, Kuwana M. Pathogenesis of systemic sclerosis: recent insights of molecular and cellular mechanisms and therapeutic opportunities. J Scleroderma Relat Disord 2017;2:137–52.

4 Matucci-Cerinic M, Kahaleh B, Wigley FM. Review: evidence that systemic sclerosis is a vascular disease. Arthritis Rheum 2013;65:1953–62.

5 Denton CP, Khanna D. Systemic sclerosis. Lancet 2017; 390:1685–99.

6 Rosa I, Romano E, Fioretto BS, Manetti M. The contribution of mesenchymal transitions to the pathogenesis of systemic sclerosis. Eur J Rheumatol 2020;7:157–64.

7 Mostmans Y, Cutolo M, Giddelo C *et al.* The role of endothelial cells in the vasculopathy of systemic sclerosis: a systematic review. Autoimmun Rev 2017;16:774–86.

8 Chang X, Wei C. Glycolysis and rheumatoid arthritis: glycolysis and RA. Int J Rheum Dis 2011;14:217–22.

9 Stathopoulou C, Nikoleri D, Bertsias G. Immunometabolism: an overview and therapeutic prospects in autoimmune diseases. Immunotherapy 2019;11:813–29.

10 Zhao X, Psarianos P, Ghoraie LS *et al.* Metabolic regulation of dermal fibroblasts contributes to skin extracellular matrix homeostasis and fibrosis. Nat Metab 2019;1:147–57.

11 Xie N, Tan Z, Banerjee S *et al.* Glycolytic reprogramming in myofibroblast differentiation and lung fibrosis. Am J Respir Crit Care Med 2015;192:1462–74.

12 Bonnet S, Michelakis ED, Porter CJ *et al.* An abnormal mitochondrial–hypoxia inducible factor-1α–Kv channel pathway disrupts oxygen sensing and triggers pulmonary arterial hypertension in fawn hooded rats: similarities to human pulmonary arterial hypertension. Circulation 2006;113:2630–41.

13 Kottmann RM, Kulkarni AA, Smolnycki KA *et al.* Lactic acid is elevated in idiopathic pulmonary fibrosis and induces myofibroblast differentiation via pH-dependent activation of transforming growth factor-β. Am J Respir Crit Care Med 2012;186:740–51.

14 Castello-Cros R, Whitaker-Menezes D, Molchansky A *et al.* Scleroderma-like properties of skin from caveolin-1-deficient mice: implications for new treatment strategies in patients with fibrosis and systemic sclerosis. Cell Cycle 2011;10:2140–50.

15 Vincent AS, Phan TT, Mukhopadhyay A *et al.* Human skin keloid fibroblasts display bioenergetics of cancer cells. J Invest Dermatol 2008;128:702–9.

16 Serratì S, Cinelli M, Margheri F *et al.* Systemic sclerosis fibroblasts inhibit in vitro angiogenesis by MMP-12-dependent cleavage of the endothelial cell urokinase receptor. J Pathol 2006;210:240–8.

17 Mena HA, Zubiry PR, Dizier B *et al.* Acidic preconditioning of endothelial colony-forming cells (ECFC) promote vasculogenesis under proinflammatory and high glucose conditions in vitro and in vivo. Stem Cell Res Ther 2018;9:120.

18 Margheri F, Chillà A, Laurenzana A *et al.* Endothelial progenitor cell–dependent angiogenesis requires localization of the full-length form of uPAR in caveolae. Blood 2011;118:3743–55.

19 Manetti M, Guiducci S, Romano E *et al.* Increased serum levels and tissue expression of matrix metalloproteinase-12 in patients with systemic sclerosis: correlation with severity of skin and pulmonary fibrosis and vascular damage. Ann Rheum Dis 2012;71: 1064–72.

20 D'Alessio S, Fibbi G, Cinelli M *et al.* Matrix metalloproteinase 12-dependent cleavage of urokinase receptor in systemic sclerosis microvascular endothelial cells results in impaired angiogenesis. Arthritis Rheum 2004;50:3275–85.

21 Chillà A, Margheri F, Biagioni A *et al.* Mature and progenitor endothelial cells perform angiogenesis also under protease inhibition: the amoeboid angiogenesis. J Exp Clin Cancer Res 2018;37:74.

22 Manetti M, Romano E, Rosa I *et al.* Endothelial-to-mesenchymal transition contributes to endothelial dysfunction and dermal fibrosis in systemic sclerosis. Ann Rheum Dis 2017;76:924–34.

23 Piera-Velazquez S, Mendoza FA, Jimenez SA. Endothelial to mesenchymal transition (endoMT) in the pathogenesis of human fibrotic diseases. J Clin Med 2016;5:45.

24 Jimenez SA. Role of endothelial to mesenchymal transition in the pathogenesis of the vascular alterations in systemic sclerosis. ISRN Rheumatol 2013; 2013:1–15.

25 Karasek MA. Does transformation of microvascular endothelial cells into myofibroblasts play a key role in the etiology and pathology of fibrotic disease? Med Hypotheses 2007;68:650–5.

26 Para R, Romero F, George G, Summer R. Metabolic reprogramming as a driver of fibroblast activation in pulmonary fibrosis. Am J Med Sci 2019;357:394–8.

27 Ding H, Jiang L, Xu J *et al.* Inhibiting aerobic glycolysis suppresses renal interstitial fibroblast activation and renal fibrosis. Am J Physiol Renal Physiol 2017;313: F561–F575.

28 Chen Y, Choi SS, Michelotti GA *et al.* Hedgehog controls hepatic stellate cell fate by regulating metabolism. Gastroenterology 2012;143:1319–29.e11.

29 Savolainen ER, Leo MA, Timpl R, Lieber CS. Acetaldehyde and lactate stimulate collagen synthesis of cultured baboon liver myofibroblasts. Gastroenterology 1984;87:777–87.

30 Murgia F, Svegliati S, Poddighe S *et al.* Metabolomic profile of systemic sclerosis patients. Sci Rep 2018;8: 7626.

31 Vadrucci M, Castellani M, Benti R. Active subcutaneous calcinosis demonstrated by fluorine-18 fluorodeoxyglucose positron emission tomography/computed tomography in a case of limited cutaneous systemic sclerosis. Indian J Nucl Med 2016;31:154.

32 Oksuzoglu K, Ozen G, Inanir S, Direskeneli R. Flip-flop phenomenon in systemic sclerosis on fluorodeoxyglucose positron emission tomography/ computed tomography. Indian J Nucl Med 2015;30:350.

33 Nishiyama Y, Yamamoto Y, Dobashi H, Kameda T. Clinical value of ^{18}F-fluorodeoxyglucose positron emission tomography in patients with connective tissue disease. Jpn J Radiol 2010;28:405–13.

34 Lisanti MP, Martinez-Outschoorn UE, Sotgia F. Oncogenes induce the cancer-associated fibroblast phenotype: metabolic symbiosis and "fibroblast addiction" are new therapeutic targets for drug discovery. Cell Cycle 2013;12:2723–32.

35 Fiaschi T, Marini A, Giannoni E *et al.* Reciprocal metabolic reprogramming through lactate shuttle coordinately influences tumor-stroma interplay. Cancer Res 2012;72:5130–40.

36 Di Pompo G, Lemma S, Canti L *et al.* Intratumoral acidosis fosters cancer-induced bone pain through the activation of the mesenchymal tumor-associated stroma in bone metastasis from breast carcinoma. Oncotarget 2017;8:54478–96.

37 Faes S, Uldry E, Planche A *et al.* Acidic pH reduces VEGF-mediated endothelial cell responses by downregulation of VEGFR-2; relevance for anti-angiogenic therapies. Oncotarget 2016;7:86026–38.

38 Mena HA, Lokajczyk A, Dizier B *et al.* Acidic preconditioning improves the proangiogenic responses of endothelial colony forming cells. Angiogenesis 2014; 17:867–79.

39 Lee JY, Onanyan M, Garrison I *et al.* Extrinsic acidosis suppresses glycolysis and migration while increasing network formation in pulmonary microvascular endothelial cells. Am J Physiol Lung Cell Mol Physiol 2019;317:L188–L201.

40 Marcu R, Choi YJ, Xue J *et al.* Human organ-specific endothelial cell heterogeneity. iScience 2018;4:20–35.

41 Fischer H. Function of proton channels in lung epithelia. Wiley Interdiscip Rev Membr Transp Signal 2012;1: 247–58.

42 Massip-Copiz MM, Santa-Coloma TA. Extracellular pH and lung infections in cystic fibrosis. Eur J Cell Biol 2018;97:402–10. https://doi.org/10.1016/j.ejcb.2018.06.001

43 Rosso MD, Margheri F, Serrati S *et al.* The urokinase receptor system, a key regulator at the intersection between inflammation, immunity, and coagulation. Curr Pharm Des 2011;17:1924–43.

44 Montuori N, Ragno P. Role of uPA/uPAR in the modulation of angiogenesis. Chem Immunol Allergy 2014;99:105–22.

45 Kanno Y. The role of fibrinolytic regulators in vascular dysfunction of systemic sclerosis. Int J Mol Sci 2019;20: 619.

46 Manetti M, Rosa I, Milia AF *et al.* Inactivation of urokinase-type plasminogen activator receptor (uPAR) gene induces dermal and pulmonary fibrosis and peripheral microvasculopathy in mice: a new model of experimental scleroderma? Ann Rheum Dis 2014;73:1700–9.

47 Kanno Y, Kaneiwa A, Minamida M *et al.* The absence of uPAR is associated with the progression of dermal fibrosis. J Invest Dermatol 2008;128:2792–7.

48 Ojoo JC, Mulrennan SA, Kastelik JA *et al.* Exhaled breath condensate pH and exhaled nitric oxide in allergic asthma and in cystic fibrosis. Thorax 2005;60: 22–6.

49 Tate S, MacGregor G, Davis M *et al.* Airways in cystic fibrosis are acidified: detection by exhaled breath condensate. Thorax 2002;57:926–9.

50 Jones KM, Randtke EA, Howison CM *et al.* Measuring extracellular pH in a lung fibrosis model with acidoCEST MRI. Mol Imaging Biol 2015;17:177–84.